

## Article

# Zircon U–Pb Dating and Geochemical Characteristics of Chahannuo Gabbros in the Northern Margin of Qaidam Basin, Northern Tibetan Plateau

Wei Du <sup>1,2</sup>, Lei Pei <sup>1,2</sup>, Ruibao Li <sup>1,2</sup>, Zuo Chen Li <sup>1,2</sup> , Chengjun Liu <sup>1,2</sup>, Mao Wang <sup>1</sup>, Hao Lin <sup>1</sup> and Xianzhi Pei <sup>1,2,\*</sup><sup>1</sup> School of Earth Science and Resources, Chang'an University, Xi'an 710054, China; xaduwei@163.com (W.D.)<sup>2</sup> Key Laboratory of Western China's Mineral Resources and Geological Engineering, Chang'an University, Xi'an 710054, China

\* Correspondence: peixzh@163.com

**Abstract:** Late Paleozoic–early Mesozoic intrusive rocks are distributed widely along the northern margin of the Qaidam Basin in the northern Tibetan Plateau. To constrain the tectonic evolution, we carried out petrological, chronological, and geochemical studies of the Chahannuo gabbros. LA-ICP-MS Zircon U–Pb dating yields an age of  $255.0 \pm 0.9$  Ma for the gabbros, which confirms the existence of Indosinian tectono-magmatic activity on the northern margin of the Qaidam Basin. The Chahannuo gabbros have low whole-rock  $\text{SiO}_2$ ,  $\text{Fe}_2\text{O}_3$  contents, and high  $\text{Al}_2\text{O}_3$  contents, which suggests a calc-alkaline affinity. In addition, the gabbros have high MgO, Cr, and Ni contents and  $\text{Mg}^\#$ , similar to those predicted of the regional basaltic melts, and indicating that they were affected mainly by fluid from the subducted slab. The Chahannuo gabbros are characterized by arc-like trace element patterns, with enrichment in LREE and LILE, and depletion in HREE and HFSE. No obvious negative Eu anomalies also indicate that no significant magmatic differentiation has occurred. The low Nb/La ratio and Ti content in gabbros samples suggests that the Chahannuo gabbros were partially contaminated by the crust during their formation. The Chahannuo gabbros have high incompatible element ratios (Rb/Sr, Th/Nd, and Th/La), which are closer to the category of enriched mantle. Combining our data with previous data from contemporaneous magmatism in the region, we suggest that the Chahannuo gabbros formed in a continental arc environment related to the northward subduction of the Paleo-Tethyan oceanic plate.

**Keywords:** northern margin of Qaidam Basin; Indosinian; gabbros; zircon U–Pb dating; geochemistry

**Citation:** Du, W.; Pei, L.; Li, R.; Li, Z.; Liu, C.; Wang, M.; Lin, H.; Pei, X. Zircon U–Pb Dating and Geochemical Characteristics of Chahannuo Gabbros in the Northern Margin of Qaidam Basin, Northern Tibetan Plateau. *Minerals* **2023**, *13*, 651. <https://doi.org/10.3390/min13050651>

Academic Editor: Manuel Francisco Pereira

Received: 20 March 2023

Revised: 5 May 2023

Accepted: 6 May 2023

Published: 9 May 2023



**Copyright:** © 2023 by the authors. Licensee MDPI, Basel, Switzerland. This article is an open access article distributed under the terms and conditions of the Creative Commons Attribution (CC BY) license (<https://creativecommons.org/licenses/by/4.0/>).

## 1. Introduction

The northern margin of the Qaidam Basin is a multicycle orogenic system located on the northern margin of the Tibetan Plateau (Figure 1) [1–3]. The Caledonian and Himalayan tectonic movements had a significant impact on the tectonic evolution process of the northern margin of Qaidam. The Precambrian metamorphic basement in the northern margin of Qaidam is mainly composed of the Paleoproterozoic Dakendaban Group and the Middle Neoproterozoic tonalite monzogranitic gneiss. In the middle and late Neoproterozoic, the northern margin of Qaidam underwent the breakup of the Rodinia supercontinent and the opening and expansion of the South Qilian Ocean. From ca. 540 to 446 Ma, the South Qilian Ocean subducted northward to the Qilian Block, and the northern margin of Qaidam was in the stage of ocean subduction, island arc, and back arc basin evolution. The stage of ocean basin closing and continental deep subduction was during ca. 445–420 Ma. At ca. 420–400 Ma, subduction, exhumation, and orogeny began, followed by post-orogenic compression, extension, and denudation. The molasse of the Devonian Wasiushan Formation marks the end of the Caledonian orogeny [4–12]. However, the geologic history of the northern margin of the Qaidam Basin and the neighboring orogens during the late Hercynian–Indosinian still remains poorly constrained, due to the paucity of

tectonothermal signatures preserved during a magmatic [7,13–18]. Some researchers have suggested that the tectonic setting of the Qaidam Basin during the late Paleozoic–Mesozoic involved the northward subduction and collision of the Anyimaqen–Mianlue Ocean [15,19], some have suggested break-off of the Paleo-Tethyan slab in the post-collision stage [20,21], and others have proposed the northward subduction and collision of the Qinling–Qilian tectonic belt [13,22].

The northern margin of the Qaidam Basin, representing the junction between the Qinling–Qilian and East Kunlun tectonic belts, is a key area for studying the late Hercynian–Indosinian geotectonics and evolution of the Paleo-Tethys [23]. The object of this study are the Chahannuo gabbros, located in the most well exposed area of the Carboniferous–Triassic rocks from the eastern part of the northern margin of the Qaidam Basin. Here, we report original petrological, zircon U–Pb ages, and whole-rock geochemical data of the Chahannuo gabbros to provide insights into the late Paleozoic–early Mesozoic tectonic evolution of the northern margin of the Qaidam Basin.

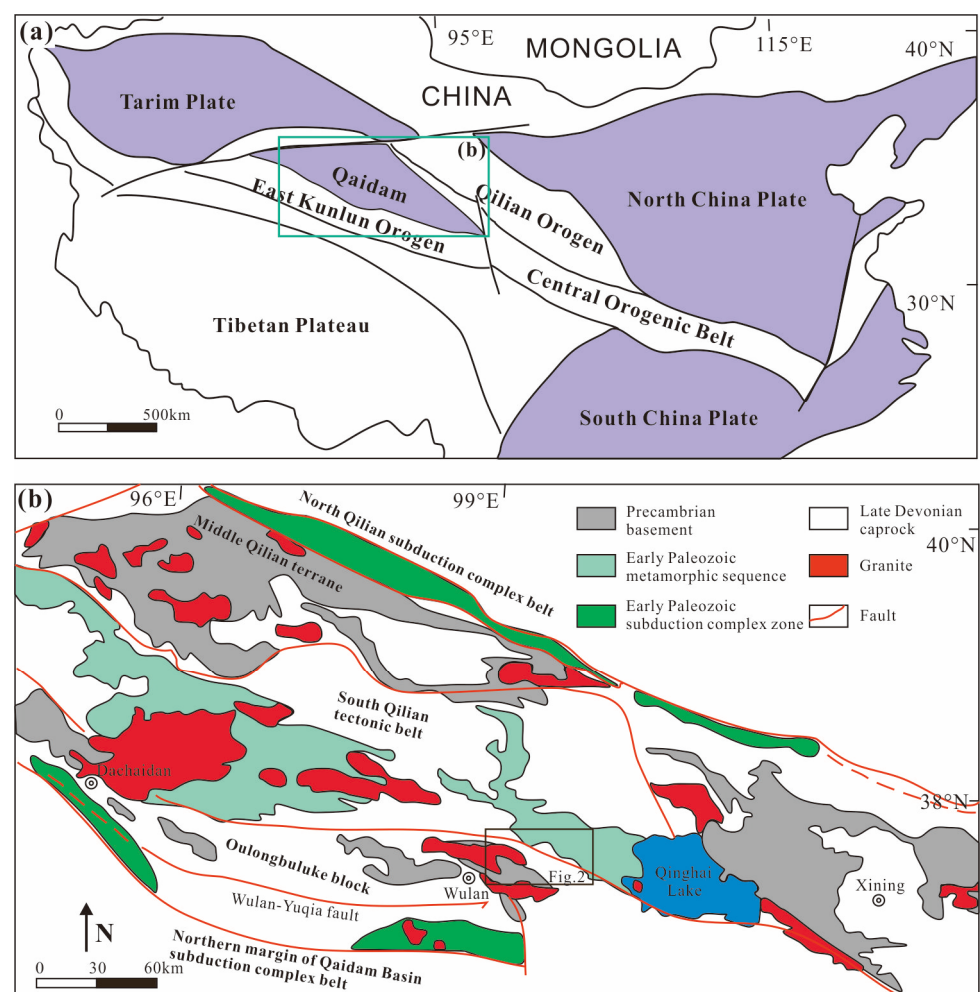


**Figure 1.** Tectonic framework of the Central China Orogen (a), modified from [24]; and geological map of the northern margin of Qaidam Basin (b), modified after [25].

## 2. Regional Geological Setting

The northern margin of the Qaidam Basin is located on the northern side of the Qaidam Block. The western end is truncated by the AltynTagh strike-slip Fault and the eastern end by the Wahongshan Fault. To the north, the basin is separated from the South Qilian orogenic belt by the Qinghai Nanshan Fault [26–29]. Tectonically, it consists of several units that strike E–W (Figure 1). From south to north, the northern margin of the Qaidam Basin

can be divided into an early Paleozoic subduction zone, the Oulongbuluke Block, and the Zongwulong tectonic zone [1,15,26,28,30,31].

The early Paleozoic Qaidam subduction zone exposed rocks that date from the Proterozoic to the late Paleozoic, including the Dakendaban Group, the Shaliuhe Group, the Tanjianshan Group, and the Yaniushan Formation [5,26,32]. The Oulongbuluke Block is composed mainly of the Dakendaban Group, the Delingha Complex, the Wandonggou Group, and the Nanhua–Sinian Quanji Group. The northeastern part of the Oulongbuluke Block underwent high amphibolite to granulite facies metamorphism and melting at depth during the early Paleozoic [33–37], and many early Paleozoic and late Paleozoic–Mesozoic intrusive rocks were exposed [9,11,14,38]. The Zongwulong tectonic belt is composed mainly of the Dakendaban Group, the Carboniferous Zongwulong Group, the Early–Middle Triassic Junzihe Group, Indosinian granite, and island arc volcanic rocks [15,39].

Strong magmatic activity in the northern margin of the Qaidam Basin, mainly consisted of intermediate-acid rocks. The late Hercynian–Indosinian igneous rock mainly consisted of late Permian–middle Triassic gabbros and calc alkaline I-type granite, and a small amount of late Triassic A-type granite. The surrounding rock are mainly amphibolite, gneiss, migmatite, granulite, quartz schist, phyllite, and marble, and no obvious metasomatism and thermal metamorphism is found at the contact boundary. In the adjacent western Qinling and eastern Kunlun regions, Triassic intermediate-acid volcanic rocks and granite are widely developed, and together formed the igneous rock belt closely related to the evolution of the Paleo-Tethys Ocean. In the western Qinling, there are mainly calc alkaline-high potassium calc alkaline granodiorite and Late Triassic basalt, andesite, dacite, and rhyolite. The arc-type granite closely related to subduction is developed in the East Kunlun region, mainly consisting of a combination of monzogranite and potassium feldspar granite.

Gabbros samples were collected from the Chahannuo area in the eastern part of the Oulongbuluke Block (Figure 2). The Chahannuo gabbros (Figure 3a,b) are exposed over ~6 km<sup>2</sup> and were emplaced into Neoproterozoic–early Paleozoic gneisses. They consist of plagioclase, pyroxene, and amphibole (Figure 3c,d). The main accessory minerals are apatite, zircon, and titanite. Plagioclase crystals are subhedral to euhedral, 1–3 mm in length, and show a poikilitic texture. Plagioclase is occasionally sericitized. The pyroxene crystals are 0.5–3 mm in length, and exist as a subhedral granular texture.

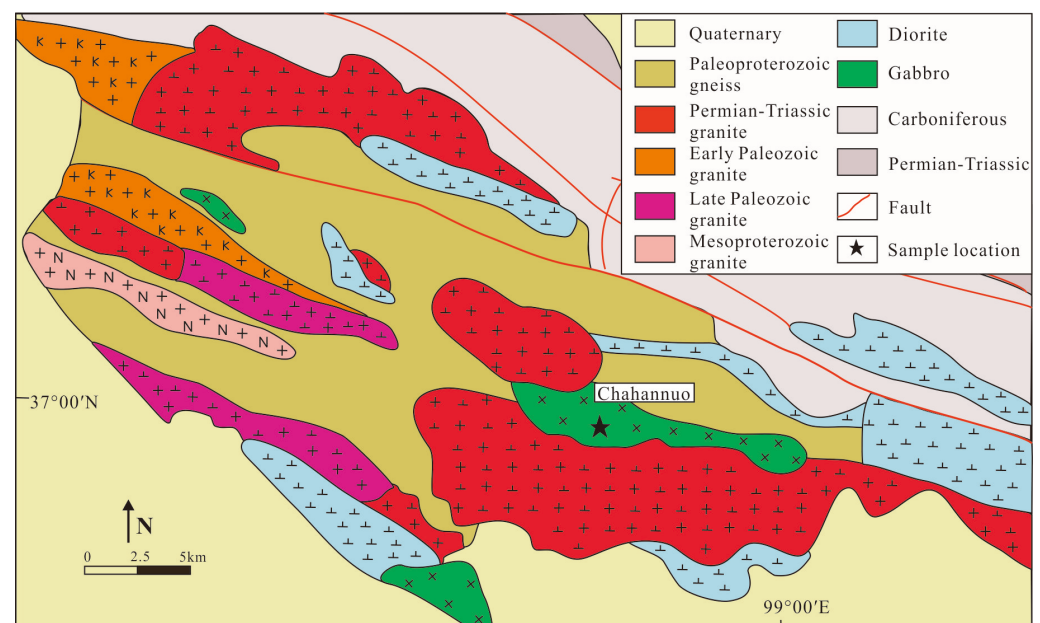


**Figure 2.** Geological sketch map of the Chahannuo and adjacent area.

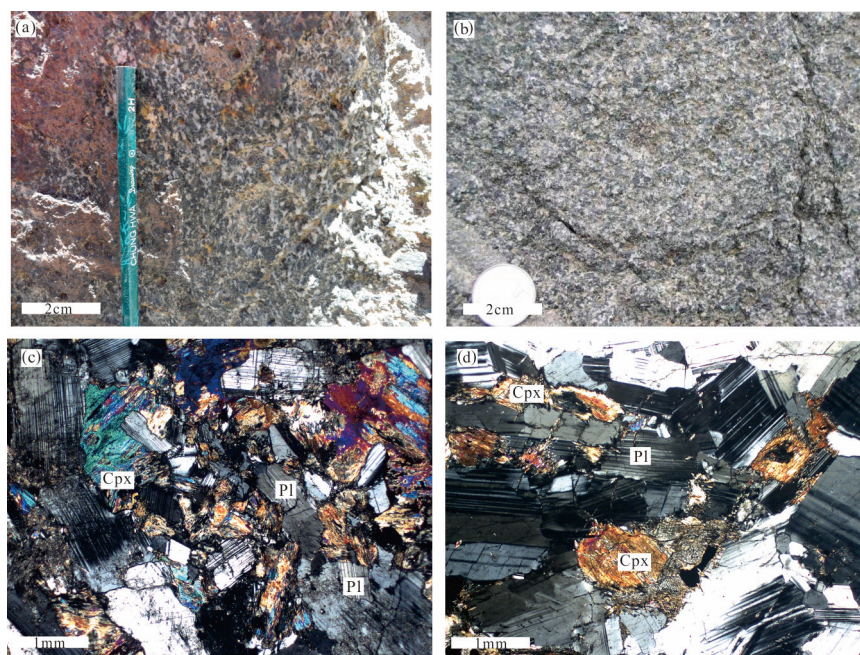


**Figure 3.** Outcrops and photomicrographs of Chahannuo gabbros. The rocks show a medium-fine gabbroic texture (a,b); and Photomicrograph of gabbros (c,d) (cross-polarized light). Abbreviations: Cpx, clinopyroxene; Pl, plagioclase.

### 3. Analytical Methods

#### 3.1. Major and Trace Elements

In the geochemical analysis, samples were crushed and milled to  $\sim 80 \mu\text{m}$  and surface alteration was removed. Before testing, acid digestion of samples in Teflon bombs was conducted. The instruments used were X-ray fluorescence (XRF; 1500) and ICP-MS (Element II), respectively. These measurements were conducted at the Institute of Geology and Geophysics, Chinese Academy of Sciences. USGS and Chinese national rock (BCR-2, GSR-1, and GSR-3) were used as test standards. The analytical precision and accuracy of the major elements were better than 5% and for most of the trace elements were better than 2%. The detailed analytical procedures were described in [40].

#### 3.2. Zircon U–Pb Dating

LA-ICP-MS zircon U–Pb experiments were conducted at the State Key Laboratory of Continental Dynamics, Northwest University, Xi’an, China. The zircons were separated by flotation and electromagnetic methods. Handpicking of zircons occurred under a binocular microscope, and they were mounted in epoxy resin, using standard heavy liquid and magnetic techniques to separate them, and the sample mount was polished. The FEI PHILIPS XL30 SFEG instrument was used to document the internal zircon structures by cathodoluminescence. Test conditions: with 2 min scanning time at 15 kV and 120 nA. This method assisted with the interpretation of the U–Pb data [41,42].

Zircon U–Pb dating was performed using an ICP-MS (Agilent 7500a) and an excimer laser ablation system (193 nm, GeoLas 200 M, Lambda Physic). The NIST SRM-610 standard glass was used as standard minerals for instrument calibration. The external reference materials and internal standard for zircon dating and element analyses were He stream and  $^{29}\text{Si}$ , respectively. The isotopic ratios and element concentrations of zircons were calculated using the Glitter software (ver. 4.0, Macquarie University), and concordia ages and diagrams were obtained using Isoplot/Ex (ver. 2.94) [43].

### 4. Results

#### 4.1. Whole-Rock Geochemistry

The whole-rock major and trace element contents are listed in Table 1. The Chahannuo gabbros have low SiO<sub>2</sub> (51.16–53.01 wt.%), P<sub>2</sub>O<sub>5</sub> (0.03–0.34 wt.%), TiO<sub>2</sub> (0.40–0.99 wt.%), and total Fe<sub>2</sub>O<sub>3</sub> (6.43–8.92 wt.%) contents, and high Al<sub>2</sub>O<sub>3</sub> (9.09–13.38 wt.%) contents (Table 1). On a total alkali versus silica (TAS) classification diagram (Figure 4a), they plot in the gabbroic diorite field. In the Nb/Y vs. Zr/TiO<sub>2</sub> diagram, the sample falls into the basalt region (Figure 4b). The low total alkali contents (ALK = 2.15–4.65 wt.%) and Rittmann index values ( $\sigma = 0.56$ –2.49) indicate that the Chahannuo gabbros are subalkaline. On a K<sub>2</sub>O versus SiO<sub>2</sub> diagram (Figure 4c) and AFM diagram (Figure 4d), the samples plot along the subalkaline series and show a calc-alkaline affinity.

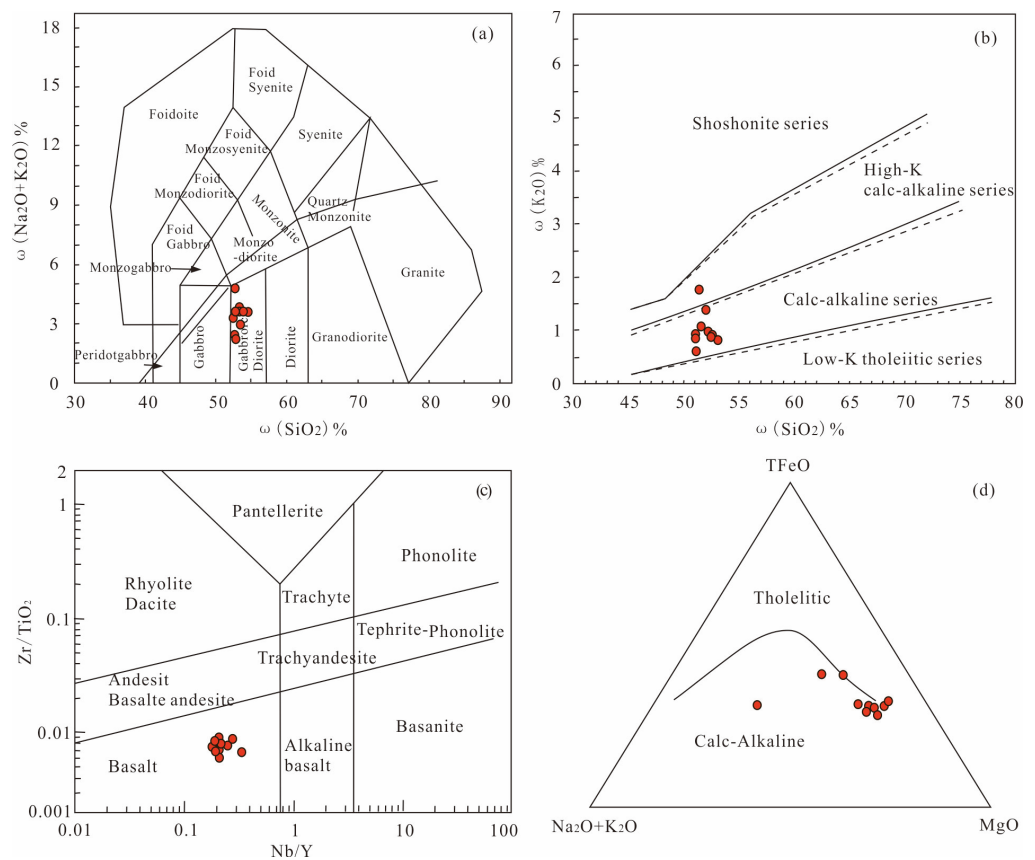


**Figure 4.** Total alkali vs. silica (TAS) (a); K<sub>2</sub>O vs. SiO<sub>2</sub> (b); Zr/TiO<sub>2</sub> vs. Nb/Y (c); and TFeO-Na<sub>2</sub>O + K<sub>2</sub>O-MgO diagrams (d), modified from [44,45] for Chahannuo gabbros samples.

**Table 1.** Major (wt.%) and trace element (ppm) data for Chahannuo gabbros.

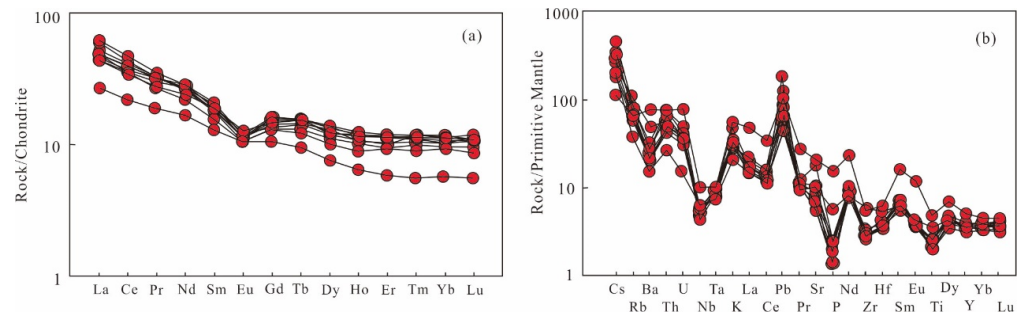
Sample	CHR01	CHR02	CHR03	CHR04	CHR05	CHR06	CHR07	CHR08	CHR09	CHR10
SiO <sub>2</sub>	52.48	52.01	52.68	53.01	51.26	51.16	51.66	52.36	51.28	51.68
TiO <sub>2</sub>	0.52	0.46	0.41	0.41	0.53	0.56	0.54	0.40	0.76	0.99
Al <sub>2</sub> O <sub>3</sub>	10.02	10.66	12.04	11.43	9.09	9.16	9.81	13.25	13.70	13.38
TFe <sub>2</sub> O <sub>3</sub>	7.42	7.38	6.43	6.92	8.82	8.78	7.66	6.38	8.92	8.82
MnO	0.12	0.12	0.11	0.13	0.14	0.14	0.12	0.12	0.16	0.16
MgO	14.01	14.19	11.87	12.36	15.20	15.05	14.59	10.85	9.34	8.28
CaO	11.03	9.71	11.69	10.22	10.13	10.43	10.29	11.23	10.23	10.23
Na <sub>2</sub> O	1.86	1.93	2.49	2.42	1.26	1.31	2.04	2.53	2.47	2.93
K <sub>2</sub> O	0.94	1.41	0.92	0.85	0.89	0.91	1.07	0.99	0.64	1.72
P <sub>2</sub> O <sub>5</sub>	0.05	0.03	0.04	0.05	0.03	0.03	0.04	0.05	0.12	0.34

Table 1. Cont.

Sample	CHR01	CHR02	CHR03	CHR04	CHR05	CHR06	CHR07	CHR08	CHR09	CHR10
LOI	1.68	2.07	1.25	2.33	2.61	2.41	2.30	1.62	2.12	1.37
TOTAL	100.13	99.97	99.93	100.13	99.96	99.94	100.12	99.78	99.74	99.90
FeO	5.61	5.09	4.38	5.02	6.18	5.78	5.61	4.38	5.75	5.89
Mg <sup>#</sup>	78.90	79.20	78.53	77.96	77.34	77.25	79.05	77.11	67.47	65.03
A/NK	3.58	3.19	3.53	3.50	4.23	4.13	3.15	3.76	4.41	2.88
A/CNK	0.72	0.82	0.80	0.85	0.74	0.72	0.73	0.90	1.03	0.90
A/MF	0.47	0.49	0.66	0.59	0.38	0.38	0.44	0.77	0.75	0.78
C/MF	0.51	0.45	0.64	0.53	0.42	0.44	0.46	0.65	0.56	0.60
Sc	38.50	32.76	36.88	33.38	39.08	39.00	36.94	32.32	35.29	29.90
Co	48.93	52.70	39.99	36.16	66.29	63.78	55.03	37.64	37.33	37.32
Ni	154.54	167.53	121.13	101.36	179.90	170.90	194.38	87.10	46.31	69.62
Cu	7.20	23.34	32.62	12.95	42.42	39.97	19.92	12.75	18.26	17.34
Zn	56.65	62.17	48.64	54.68	71.74	67.22	64.19	53.17	77.48	88.26
Ga	10.26	10.58	12.34	11.20	11.15	10.94	10.86	13.50	14.25	15.63
Rb	52.31	69.38	54.20	43.47	39.24	39.45	50.59	45.34	24.76	43.91
Sr	163.44	182.00	212.21	362.05	118.31	115.57	143.77	211.87	214.89	422.45
Y	16.94	15.92	15.35	16.28	16.45	17.04	17.66	13.34	16.08	22.54
Zr	35.94	32.50	30.54	35.09	29.86	28.87	34.27	29.71	65.79	58.64
Nb	3.97	3.41	3.92	3.54	3.81	3.88	3.99	2.93	4.31	6.84
Mo	0.10	0.09	0.23	0.10	0.18	0.10	0.15	0.18	0.10	0.22
Sn	1.66	1.86	1.30	1.30	1.39	1.47	1.64	1.11	1.02	3.74
Cs	2.69	1.66	3.49	1.99	1.47	1.45	2.33	2.54	1.58	0.89
Ba	171.56	324.76	224.24	172.29	146.06	146.80	189.40	145.08	105.49	537.32
La	11.45	12.49	13.97	14.71	10.47	10.22	11.55	11.45	10.15	32.24
Ce	23.90	24.93	26.46	28.18	21.99	21.74	24.19	21.94	20.44	61.01
Pr	3.05	3.06	3.09	3.32	2.87	2.85	3.03	2.56	2.57	7.60
Nd	12.43	12.12	11.86	12.97	12.49	12.52	13.27	10.28	11.24	31.65
Sm	3.00	2.80	2.67	2.83	2.77	3.07	3.16	2.41	2.82	7.04
Eu	0.66	0.67	0.61	0.70	0.66	0.64	0.68	0.62	0.74	1.98
Gd	3.09	2.96	2.65	2.73	3.25	3.17	3.31	2.72	2.92	6.91
Tb	0.58	0.54	0.49	0.52	0.56	0.58	0.59	0.46	0.57	1.07
Dy	3.05	3.25	2.83	2.91	3.27	3.36	3.49	2.56	3.09	5.15
Ho	0.67	0.60	0.57	0.61	0.65	0.68	0.71	0.52	0.65	0.89
Er	1.85	1.71	1.56	1.65	1.89	1.89	1.94	1.55	1.84	2.35
Tm	0.28	0.26	0.25	0.30	0.28	0.29	0.30	0.23	0.29	0.33
Yb	1.73	1.72	1.63	1.96	1.83	2.02	1.89	1.59	1.89	2.24
Lu	0.29	0.27	0.24	0.27	0.27	0.28	0.30	0.22	0.27	0.32
Hf	1.21	1.12	1.05	1.22	1.09	1.15	1.32	1.13	1.62	1.96
Ta	0.38	0.35	0.39	0.39	0.35	0.33	0.37	0.33	0.30	0.40
Pb	3.85	8.54	6.17	5.61	3.21	3.13	4.59	4.52	13.01	7.29
Bi	0.27	0.29	0.21	0.17	0.12	0.11	0.24	0.11	0.23	0.11
Th	3.98	4.98	6.60	6.69	4.04	3.66	5.59	4.48	2.28	6.56
U	0.87	0.78	0.99	0.84	0.71	0.65	0.75	0.76	0.31	1.57
δEu	0.66	0.71	0.70	0.77	0.67	0.62	0.64	0.74	0.79	0.86
∑REE	66.02	67.38	68.87	73.67	63.25	63.32	68.42	59.10	59.50	160.75
LREE	54.47	56.08	58.65	62.71	51.25	51.04	55.88	49.26	47.97	141.50
HREE	11.55	11.30	10.22	10.96	12.00	12.27	12.54	9.84	11.53	19.25

The chondrite-normalized rare earth element (REE) and primitive mantle-normalized immobile trace element patterns of the samples are illustrated in Figure 5. All of the samples have similar REE and trace element patterns, indicating that they have the same magmatic source. The total amount of rare earth elements (REE) in the sample was relatively low, where LREE content ranged from 49.26 ppm to 141.50 ppm, HREE content ranged from 9.84 ppm to 19.25 ppm, and the LREE/HREE ratio was from 4.16 to 7.35. The enrichment of LREE and weak fractionation of middle and heavy REEs (Figure 5a) was similar to typical island arc magmas [46]. There were only weak negative Eu anomalies in the gabbros, indicating that weak plagioclase separation crystallization occurred during the

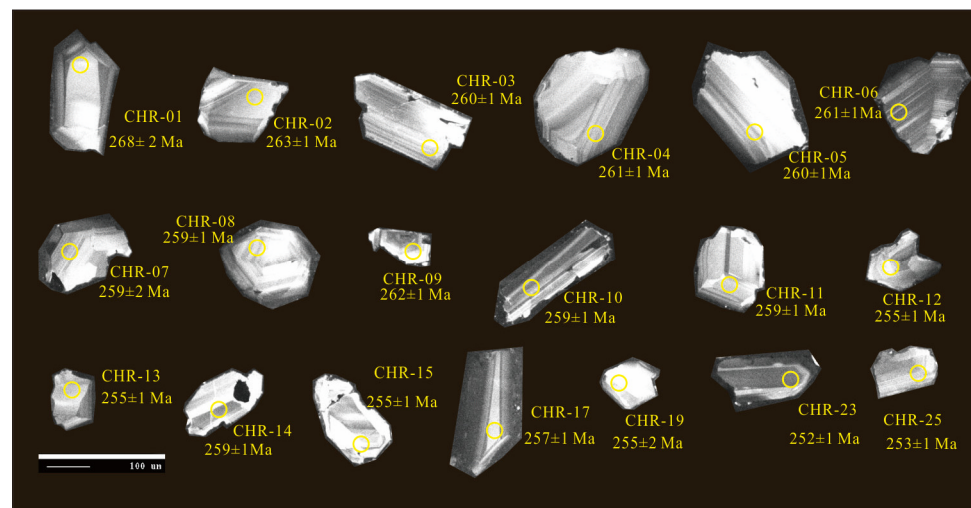
rock evolution process. On a primitive mantle-normalized trace element spider diagram, the samples showed enrichment in large ion lithophile elements (LILEs; e.g., Sr, Rb, Ba, U, and K) and depletion in high field strength elements (HFSEs; e.g., Nb, Ta, and Ti; Figure 5a), which are similar to those of island arc magmas [47,48].



**Figure 5.** Chondrite-normalized rare earth element distribution patterns (a) and primitive mantle-normalized trace element spider diagrams (b); normalization values are from [49,50].

#### 4.2. Zircon U–Pb Age

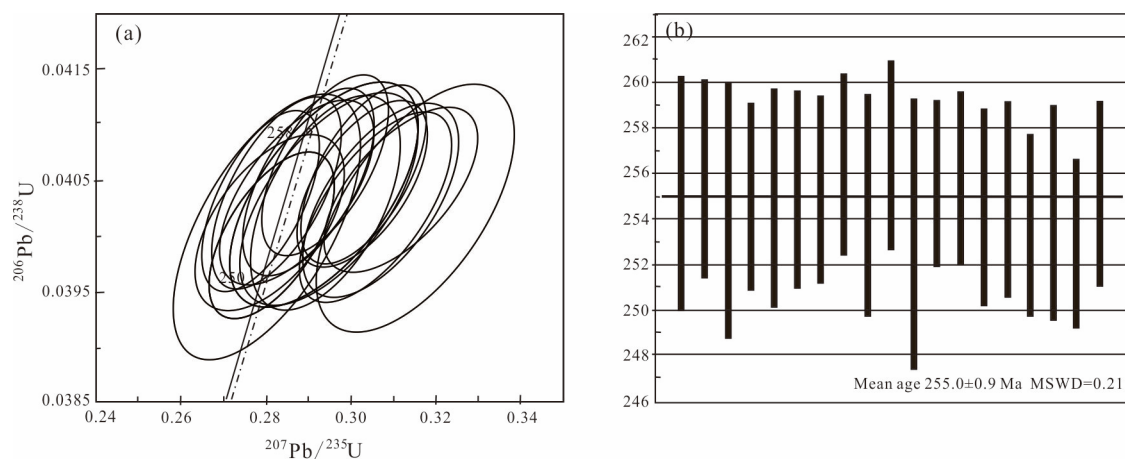
Zircon U–Pb results are listed in Table 2. Most zircon grains from the Chahannuo gabbros are colorless to pale brown, euhedral to subhedral, and 100–200  $\mu\text{m}$  long with shape ratios of 1:1–2:1 (Figure 6). Most grains display clear oscillatory and concentric zoning, and many grains show convoluted and truncated zoning. These features, together with their high Th/U ratios (mostly  $> 0.4$ ), indicate a magmatic origin [51–56]. To ensure the accuracy of the ages, analysis points were selected within the oscillatory zones. Most analyses plot on or near the concordia, yielding a weighted mean  $^{206}\text{Pb}/^{238}\text{U}$  age of  $255.0 \pm 0.9$  Ma (late Permian; Figure 7).



**Figure 6.** Cathodoluminescence (CL) images of analyzed zircon grains showing internal structures and ages.  $^{206}\text{Pb}/^{238}\text{U}$  ages are shown in parentheses.

**Table 2.** U–Pb isotopic composition of zircons in Chahannuo gabbros.

Spots	Pb (ppm)	Th (ppm)	U (ppm)	Th/U	$^{207}\text{Pb}/^{235}\text{U}$		$^{206}\text{Pb}/^{238}\text{U}$		$^{207}\text{Pb}/^{235}\text{U}$		$^{206}\text{Pb}/^{238}\text{U}$		Concordance
					Ratios	$1\sigma$	Ratios	$1\sigma$	(Ma)	$1\sigma$	(Ma)	$1\sigma$	
CHR.01	31.42	160	178.49	0.90	0.29234	0.00972	0.04152	0.00033	260	7	262	2	0.97
CHR.02	54.56	317.79	311.78	1.02	0.31248	0.00711	0.04124	0.00027	276	5	261	2	0.98
CHR.03	37.03	240.97	219.14	1.10	0.31727	0.00823	0.03981	0.00029	280	7	252	2	0.91
CHR.04	64.37	233.28	376.31	0.62	0.28439	0.00654	0.04027	0.00026	254	5	255	2	0.97
CHR.05	33.93	249.66	198.45	1.26	0.2979	0.00999	0.04023	0.00034	265	6	254	2	0.97
CHR.06	67.15	531.73	391.01	0.80	0.27972	0.00649	0.04035	0.00026	250	5	255	2	0.98
CHR.07	35.82	168.68	209.90	0.80	0.28304	0.01055	0.04008	0.00036	253	6	253	2	0.99
CHR.08	63.87	313.97	371.60	0.84	0.29304	0.00762	0.04034	0.00029	261	5	255	2	0.95
CHR.09	43.60	183.06	250.63	0.73	0.29614	0.00894	0.0408	0.00032	263	5	258	2	0.97
CHR.10	121.44	1088.82	709.90	1.53	0.300	0.00541	0.0401	0.00023	266	5	253	1	0.98
CHR.11	48.95	324.03	282.97	1.15	0.27736	0.00853	0.04048	0.00032	249	7	256	2	0.99
CHR.12	75.16	382.32	440.99	0.87	0.28429	0.01015	0.03969	0.00028	254	6	251	2	0.94
CHR.13	97.80	395.41	572.08	0.69	0.29764	0.00613	0.03995	0.00025	265	5	253	2	0.95
CHR.14	62.27	449.23	358.50	1.25	0.29824	0.00822	0.04057	0.0003	265	5	256	2	0.94
CHR.15	50.52	242.88	293.62	0.83	0.29687	0.0094	0.04017	0.00033	264	6	254	2	0.94
CHR.17	52.27	286.78	301.36	0.95	0.27754	0.00894	0.04042	0.00033	249	6	255	2	0.99
CHR.19	51.68	301.35	298.25	1.01	0.29736	0.01121	0.04033	0.00038	264	7	255	2	0.95
CHR.23	101.60	595.31	588.97	1.01	0.28238	0.00695	0.04003	0.00028	253	5	253	2	0.99
CHR.25	122.96	546.39	704.46	0.78	0.29882	0.00617	0.04046	0.00025	265	5	256	2	0.99

**Figure 7.** LA-ICP-MS zircon U–Pb concordia diagrams of the gabbros (a); and weighted average ages (b) from Chahannuo area.

## 5. Discussion

### 5.1. Crustal Contamination

Crustal contamination often occurs during magmatic evolution and emplacement [57–59]. The Chahannuo gabbros have low Ce/Pb (1.57–3.90), Nb/U (3.89–13.80), and Nb/Ta (8.87–16.94) ratios, which are lower than those of MORB, OIB, and chondrites (Ce/Pb =  $25 \pm 5$ , Nb/U =  $47 \pm 7$ , Nb/Ta =  $19.9 \pm 0.6$ ), but closer to the Ce/Pb, Nb/U, and Nb/Ta ratios of continental crust (4, 10, and 12–13, respectively) [60–62]. These features indicate the addition of crustal components.

The Chahannuo gabbros also have lower Nb/La (0.21–0.38) and Nb/Ce (0.11–0.21) ratios than the primitive mantle (1.02 and 0.4, respectively), average crust (0.69 and 0.33, respectively), and average lower crust (0.83 and 0.39, respectively) [49]. This suggests that the mafic magma did not form by mixing between crustal and mantle material. In addition, a large amount of crustal contamination will increase the LILE, Si, K<sub>2</sub>O, and Na<sub>2</sub>O contents and Nb/Ta ratios, and decrease the Mg, Ni, P<sub>2</sub>O<sub>5</sub>, and TiO<sub>2</sub> contents [59,63]; however, the Chahannuo gabbros are characterized by low Si contents and Nb/Ta ratios and high Mg and Ni contents, suggesting that they were partially contaminated by the crust during their formation.

The Ti element is not easily affected by alteration in geological processes, and negative Ti anomaly is usually considered as one of the characteristics of continental crust [59–61]. Therefore, negative Ti anomaly is often used as one of the indicators to determine whether mantle-derived magma has been contaminated by crust source. The content of TiO<sub>2</sub> in the Chahannuo gabbros is very low, showing weak negative anomalies in primitive mantle-normalized immobile trace element patterns. It also indicates that it is partially contaminated by the crust.

## 5.2. Petrogenesis and Magmatic Source

Mafic rocks, including gabbros, are usually derived from the lithospheric mantle or asthenospheric mantle [63,64]. In the Nb/Y vs. Zr/TiO<sub>2</sub> diagram, all samples of the Chahannuo gabbros fall into the basalt area, indicating that the primary magma of gabbros is basaltic magma. Some high field strength element ratios of the igneous rock chemical composition can be used to indicate the magma source area, because it is not easily affected by later hydrothermal alteration and metamorphism. This study shows that the Zr/Ba, La/Nb, and La/Ta values of the basalt source from the asthenosphere mantle are greater than 0.2, less than 1.5, and less than 22, respectively. The above ratios of basalt source from the lithospheric mantle are less than 0.2, greater than 1.5, and greater than 22, respectively. The average Zr/Ba, La/Nb, and La/Ta values of gabbros samples are 0.19, 3.35, and 17, respectively, suggesting that the magma source is from the lithospheric mantle [65]. The Chahannuo gabbros samples have high incompatible element ratios, the Rb/Sr, Th/Nd, and Th/La ratios are 0.25, 0.37, and 0.37, respectively, which are closer to the category of enriched mantle. The primary magma of the Chahannuo gabbros is enriched in MgO (8.28–15.20 wt.%), Ni (45.31–194.38 ppm), and has high Mg<sup>#</sup> (65–79), which indicates that the gabbros are derived mainly from the partial melting of mantle rocks [66]. However, the Chahannuo gabbros are enriched in LREEs and LILEs (e.g., Sr, Rb, Ba, U, and K) and depleted in HREEs and HFSEs (e.g., Nb, Ta, and Ti), which may have been caused by contamination by continental crustal material or metasomatism by subduction-derived fluid or melt [67,68]. As discussed above, the degree of contamination of the Chahannuo gabbros by crustal materials is low; therefore, metasomatism by subduction-derived fluid or melt is the most likely explanation for the arc-like geochemical characteristics of the Chahannuo gabbros.

The Chahannuo gabbros have high Th/Yb ratios (1.21–4.05), suggesting that they were affected by a subduction component [69]. Different subduction components produce arc magmas with different geochemical characteristics [70–73]. Magmas formed by fluid metasomatism often have higher LILE (e.g., Rb, Ba, and Sr), P, and U contents and thus have higher Ba/Nb, Ba/Th, and Sr/Th ratios [70–73], whereas magmas formed by melt metasomatism often have higher LREE and Th contents and Th/Ce ratios [74–78]. The Chahannuo gabbros have high Ba/Th (25.75–81.87) and Sr/Th (29.29–94.06) ratios and low Th contents (6.69–228) and Th/Ce ratios (0.11–0.25). In addition, during subduction, hydrous fluid will generally inhibit the crystallization of plagioclase, which results in negative Eu anomalies in the residual melt [79]. There are no clear negative Eu anomalies in the Chahannuo gabbros, suggesting that the fractional crystallization of plagioclase was limited. Trace element ratios (e.g., Th/Yb, Ba/La, Sr/La, and La/Yb) may indicate the input of hydrous fluid or subducted sediments. The Chahannuo gabbros samples have a narrow range of Th/Yb (1.21–4.05) and La/Yb (5.38–14.41) ratios and a wider range of Ba/La (10.39–26.01) and Sr/La (11.30–24.62) ratios. These data imply a large input of hydrous fluid to the mantle source area [80–82]. On the Th/Yb–Ba/La and Sr/La–La/Yb diagrams (Figure 8), the Chahannuo gabbros plot along a trend controlled by fluid metasomatism. In summary, the genesis of the Chahannuo gabbros is related to subduction-related metasomatism by hydrous fluid, suggesting that mafic magma may come from the partial melting of the enriched mantle.

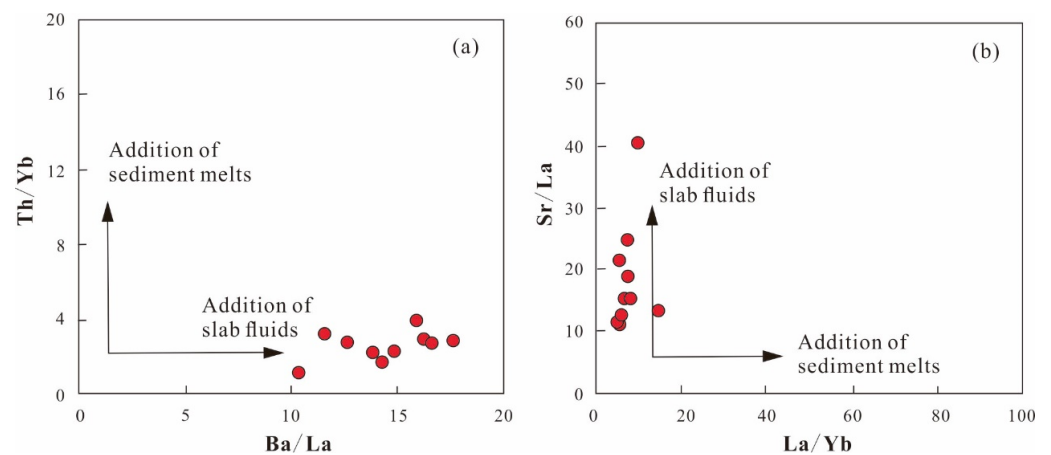


**Figure 8.** Th/Yb vs. Ba/La (a), modified from [82]); and Sr/La vs. La/Yb (b), modified from [83]) diagrams for Chahannuo gabbros samples.

### 5.3. Tectonic Environment and Geological Significance

The following hypotheses about the tectonic setting of the Indosinian magmatism on the northern margin of the Qaidam Basin have been proposed. The magma was formed during: (1) the northward subduction and collision of the Anyimaqen–Mianlue Ocean [18,19]; (2) a post-collision stage related to subduction of the Paleo-Tethyan oceanic plate [20,21]; (3) subduction and collision of the West Qinling and Qilian massifs [13,22].

The composition of rocks can be used to constrain the tectonic environment. The  $\text{TiO}_2$  content of basalts formed in different tectonic environments varies. The  $\text{TiO}_2$  content of island arc basalt is  $\sim 0.98$  wt.%, whereas those of the ridge tholeiitic basalt, island tholeiitic basalt, and intraplate are 1.5 wt.%, 2.63 wt.%, and 2.23 wt.%–2.90 wt.%, respectively. In terms of trace elements, compared to the intraplate alkaline basalt, the Nb and Ta contents of island arc basalt are very low, at  $1.7 \times 10^{-6}$ – $2.7 \times 10^{-6}$ , and  $0.1 \times 10^{-6}$ – $0.18 \times 10^{-6}$ , respectively. Moreover, the element ratios of basaltic rocks in different environments also varies. Generally, intraplate basalts and mid-ocean-ridge basalts are relatively rich in  $\text{TiO}_2$  and HFSE, and the element ratios have the following characteristics:  $\text{Nb/La} > 0.8$ ,  $\text{La/Ta} < 15$ ,  $\text{Th/Ta} < 3$ ,  $\text{Ta/Yb} < 0.1$ . The Chahannuo gabbros have low  $\text{TiO}_2$  contents (0.54 wt.%), high  $\text{Al}_2\text{O}_3$  contents, and higher  $\text{Na}_2\text{O}$  than  $\text{K}_2\text{O}$  contents. They are also enriched in LILEs (Rb, K, Sr) and depleted in HFSEs (P, Ti, Nb). On REE distribution diagrams, the LREEs are enriched and the HREEs are depleted, which is different from those of N-MORB, E-MORB, and OIB. The geochemical characteristics of Chahannuo gabbros are similar to those of typical island arc calc-alkaline basalt. In addition, the element ratios of Chahannuo gabbros, such as  $\text{La/Nb}$  (average 3.35),  $\text{Nb/La}$  (average 0.31),  $\text{La/Ta}$  (average 37.90),  $\text{Th/Ta}$  (average 13.37),  $\text{Ta/Yb}$  (average 0.20), are similar to gabbros formed in the active continental margin arc [63]. On the tectonic discrimination diagrams (Figure 9), the Chahannuo gabbros fall into the calc-alkaline volcanic rock and active continental margin regions, suggesting that they may have formed in an active continental margin environment.

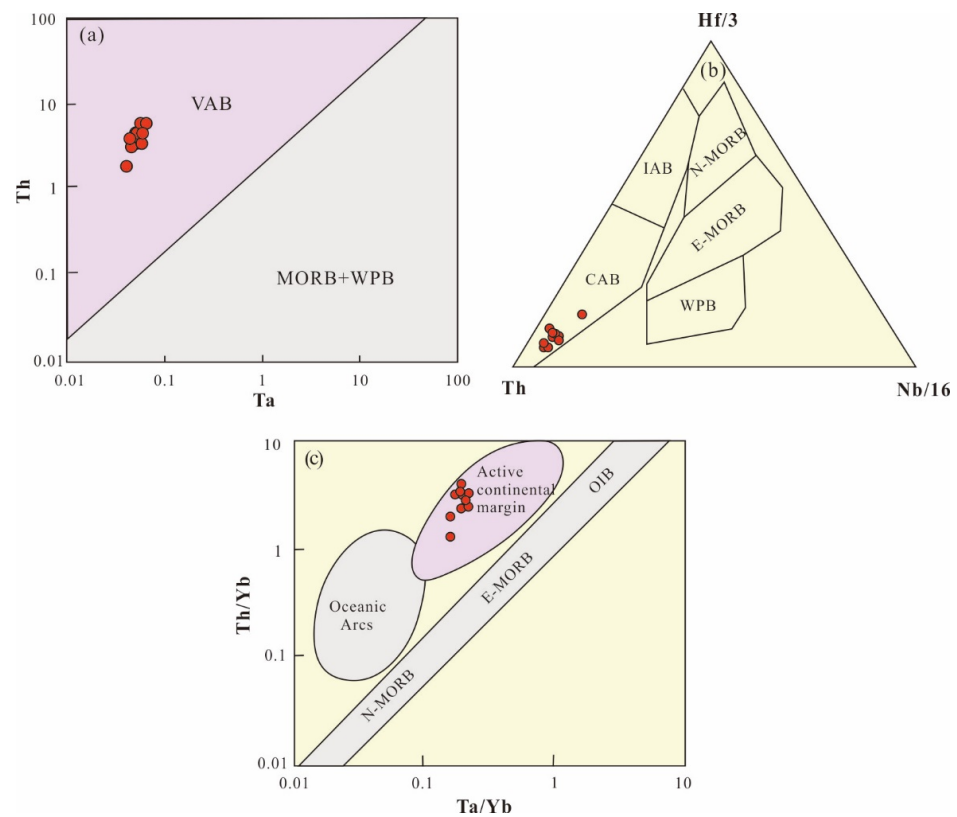


**Figure 9.** Th vs. Ta diagram (a); Hf/3–Th–Nb/16 diagram (b), modified from Wood [83]; and Th/Yb vs. Nb/Yb diagram (c), modified from [84] for Chahannuo gabbros. Abbreviations: OIB, oceanic island basalts; MORB, mid-ocean-ridge basalts; N-MORB, normal mid-ocean-ridge basalts; E-MORB, enriched mid-ocean-ridge basalts; CAB, island arc calc-alkaline basalt; IAB, island arc tholeiite basalt; WPB, within plate alkali basalt; VAB, volcanic arc basalt.

Research shows the Mesozoic igneous rock in the study area is part of the continental margin volcanic arc of the Qaidam Basin, the Early–Middle Triassic sediments are the fore-arc basin sedimentation, and the Gonghe deep-sea basin located in the east began to rise at the end of the Middle Triassic and completely disappeared in the Late Triassic. The West Qinling Mountains were mainly turbidity current deposits during the Early Middle Triassic, and transformed into shallow marine-continental deposits during the Middle Late Triassic, gradually deepening from north to south. Therefore, it is believed that there are still oceanic or deep-sea basins in the Early Middle Triassic of the Qinling–Qilian–East-Kunlun region, and the continental collision orogeny has not yet started [7]. The A-type granite related to orogenic extension and the I-type granite that formed after the early Indosinian in the eastern section of the northern margin of the Qaidam Basin suggest that the formation of the early Indosinian granite may not be related to a collisional environment [14]. The chronology and geochemistry of the Middle–Late Triassic quartz diorite porphyry and quartz porphyry on the northern side of the Anyimaqen subduction zone also suggest that they were formed in a continental arc environment [85].

In recent years, a large number of Late Permian–Middle Triassic magmatic rocks related to oceanic subduction have been found on the northern margin of the Qaidam Basin [9,10,39,86–88], including the Shaykgolai granite ( $240 \pm 2$  Ma) and granodiorite ( $249 \pm 3$  Ma), the Chahanhe granodiorite ( $240 \pm 2$  Ma), the Chahannuo granodiorite ( $242 \pm 2$  Ma), and a quartz diorite ( $252 \pm 1$  Ma) on the northern margin of the Qaidam Basin. In addition, these igneous rocks have similar geochemical characteristics with the contemporaneous active continental arc igneous rock in the East Kunlun Mountains and the West Qinling Mountains, characterized by enrichment of LREE and LILE (Rb, K, Cs), and depletion of HREE and HFSE (Nb, Ta, Ti) [19,89]. This study indicates that the Indosinian

magmatic belt in the northern margin of Qaidam and adjacent areas formed in a continental arc environment during the subduction of the Paleo-Tethyan oceanic plate.

## 6. Conclusions

1. Zircon U–Pb dating for Chahannuo gabbros yields a  $255 \pm 1$  Ma age, which indicates that it is formed in the late Permian;
2. Chahannuo gabbros are characterized by enrichment in light rare earth elements and large ion lithophile elements, and depletion in heavy rare earth elements and high field strength elements, suggesting they represent subduction-related arc magmatic rocks;
3. The northern margin of the Qaidam basin was an active continental margin in the late Permian to early Triassic. Chahannuo gabbros formed in a continental marginal arc environment related to the northward subduction of the Paleo-Tethyan oceanic plate.

**Author Contributions:** Conceptualization, X.P.; methodology, L.P.; software, H.L. and M.W.; investigation, W.D., Z.L., X.P., R.L. and L.P.; resources, X.P.; data curation, C.L.; writing—original draft preparation, W.D.; writing—review and editing, R.L. and Z.L.; supervision, X.P.; funding acquisition, W.D. and X.P. All authors have read and agreed to the published version of the manuscript.

**Funding:** This research was funded by the National Nature Sciences Foundation of China (grant numbers 42172236, 41872233, 41872235, 41502191), Natural Science Basic Research Plan in Shaanxi Province of China (grant numbers 2021JQ-241, 2019JM-312, 2019JQ-090, 2019JQ-209, 2020JM-229), the Fundamental Research Funds for the Central Universities (grant numbers 300102270107, 300102270202, 300103183081, 300103120009, 300104282717, 300102279204, 201810710233), the Commonwealth Geological Survey, the Aluminum Corporation of China and the Land-Research Department of Qinghai Province (grant number 200801), and the Youth Innovation Team of Shaanxi Universities.

**Data Availability Statement:** The original contributions presented in the study are included in the article.

**Acknowledgments:** We would like to thank the Institute of Geology and Geophysics, Chinese Academy of Sciences, and the State Key Laboratory of Continental Dynamics, Northwest University, Xi'an, China, for support and assistance on zircon U–Pb and major and trace elements analysis. The authors are grateful for the critical comments from anonymous reviewers, which profoundly enhanced the quality of this manuscript.

**Conflicts of Interest:** The authors declare no conflict of interest.

## References

1. Pan, G.T.; Li, X.Z.; Wang, L.Q.; Ding, J.; Chen, Z.L. Preliminary division of tectonic units of the Qinghai-Tibet Plateau and its adjacent regions. *Geol. Bull. China* **2002**, *21*, 701–707.
2. Xu, Z.Q.; Yang, J.S.; Li, H.B.; Zhang, J.X.; Zeng, L.S.; Jiang, M. The Qinghai-Tibet plateau and continental dynamics: A review on terrain tectonics, collisional orogenesis, and processes and mechanisms for the rise of plateau. *Geol. China* **2006**, *33*, 221–238.
3. Yin, F.H.; Zhang, K.X. Characteristics of the eastern Kunlun orogenic belt. *Earth Sci.* **1997**, *22*, 339–342.
4. Zhang, J.X.; Yang, J.S.; Mattinson, C.G.; Xu, Z.Q.; Meng, F.C.; Shi, R.D. Two contrasting eclogite cooling histories, North Qaidam HP/UHP terrane, western China: Petrological and isotope constraints. *Lithos* **2005**, *84*, 51–76. [[CrossRef](#)]
5. Wang, H.C.; Li, H.K.; Lu, S.N.; Yuan, G.B.; Xin, H.T. Geological characteristics and tectonic setting of the Dakendaha Group in Iqe area, northern margin of Qaidam Basin. *Geol. Surv. Res.* **2006**, *29*, 253–262.
6. Huang, W.; Zhang, L.; Ba, J.; Liao, F.X.; Chen, N.S. Detrital zircon LA-ICP-MS U-Pb dating for K-feldspar leptyte of Quanji massif in the north margin of Qaidam block: Constraint on the age of Dakendaban Group. *Geol. Bull. China* **2011**, *30*, 1353–1359.
7. Yan, Z.; Wang, Z.Q.; Li, J.L.; Xu, Z.Q.; Deng, J.F. Tectonic settings and accretionary orogenesis of the West Qinling terrane, northeastern margin of the Tibet Plateau. *Acta Petrol.* **2012**, *28*, 1808–1828.
8. Xu, Z.Q.; Yang, J.S.; Li, W.C.; Li, H.Q.; Cai, Z.H.; Yan, Z.; Ma, C.Q. Paleo-Tethys system and accretionary orogen in the Tibet Plateau. *Acta Petrol.* **2013**, *29*, 1847–1860.
9. Cheng, T.T.; Niu, M.L.; Wu, Q.; Xia, W.J.; Li, X.C. Petrogenesis of the Chahannuo gabbro on the northern margin of Qaidam Basin: Constraint from geochemistry, zircon U-Pb dating and Lu-Hf isotopes. *Chin. J. Geol.* **2015**, *50*, 741–755.
10. Wu, C.L.; Lei, M.; Wu, D.; Li, T.X. Zircon SHRIMP dating and genesis of granites in Wulan area of northern Qaidam. *Acta Geosci.* **2016**, *37*, 493–516.

11. Niu, M.L.; Zhao, Q.Q.; Wu, Q.; Li, X.C.; Yan, Z.; Li, J.L.; Sun, Y.; Yuan, X.Y. Magma mixing identified in the Guokeshan pluton, northern margin of the Qaidam Basin: Evidences from petrography, mineral chemistry, and whole-rock geochemistry. *Acta Petrol.* **2018**, *34*, 1991–2016.
12. Wu, C.L.; Wu, D.; Mattinson, C.; Lei, M.; Chen, H.J. Petrogenesis of granitoids in the Wulan area: Magmatic activity and tectonic evolution in the North Qaidam, NW China. *Gondwana Res.* **2019**, *67*, 147–171. [[CrossRef](#)]
13. Sun, Y.G.; Zhang, G.W.; Zheng, J.K.; Lu, X.X. Analysis of dynamic backgrounds of magmatic arc in the southeastern margin of Qaidam massif. *Geol. Miner. Resour. S. China* **2001**, *4*, 16–21.
14. Qiang, J. The Granitoids in Zongwulong Tectonic Zone in the Northeastern Margin of the Qinghai-Tibet Plateau and Its Tectonic Significance. Master's Thesis, Northwestern University, Xi'an, China, 2008.
15. Guo, A.L.; Zhang, G.W.; Qiang, J.; Sun, Y.G.; Li, G.; Yao, A.P. Indosinian Zongwulong orogenic belt on the northeastern margin of the Qinghai-Tibet Plateau. *Acta Petrol.* **2009**, *25*, 1–12.
16. Li, D.B.; Niu, M.L.; Xia, W.J.; Wu, Q.; Wang, L.L. Petrology and LA-ICP-MS zircon U-Pb age of the ore-bearing porphyry in the Walegen gold deposit at the juncture of the Qinling-Qilian-Kunlun orogens. *Geol. Bull. China* **2014**, *33*, 1055–1060.
17. Xu, X.Y.; Chen, J.L.; Gao, T.; Li, P.; Li, T. Granitoid magmatism and tectonic evolution in northern edge of the western Qinling terrane. *Acta Petrol.* **2014**, *30*, 371–389.
18. Yan, Z.; Guo, X.Q.; Fu, C.L.; Aitchison, J.; Wang, Z.; Li, J. Detrital heavy mineral constraints on the Triassic tectonic evolution of the West Qinling terrane, nw China: Implications for understanding subduction of the paleo tethyan ocean. *J. Geol.* **2014**, *122*, 591–607. [[CrossRef](#)]
19. Guo, X.Q.; Yan, Z.; Wang, Z.Q.; Wang, T.; Hou, K.J.; Fu, C.L.; Li, J.L. Middle Triassic arc magmatism along the northeastern margin of the Tibet: U-Pb and Lu-Hf zircon characterization of the Gangcha complex in the West Qinling terrane, central China. *J. Geol. Soc.* **2012**, *169*, 327–336. [[CrossRef](#)]
20. Luo, B.J.; Zhang, H.F.; Xiao, Z.Q. Petrogenesis and tectonic implications of the Early Indosinian Meiwu pluton in West Qinling, central China. *Earth Sci. Front.* **2012**, *19*, 199–213.
21. Luo, B.J.; Zhang, H.F.; Lü, X.B. U-Pb zircon dating, geochemical and Sr-Nd-Hf isotopic compositions of Early Indosinian intrusive rocks in West Qinling, central China: Petrogenesis and tectonic implications. *Contrib. Mineral. Petrol.* **2012**, *164*, 551–569. [[CrossRef](#)]
22. Tao, Z.H.; Yuan, H.X.; Liu, Q.Y.; Wang, Q.H. Geochemical characteristics and significance of the Gangcha complex in the West Qinling. *Geol. Explor.* **2014**, *50*, 543–549.
23. Liu, B.; Ma, C.; Jiang, H.; Guo, P.; Zhang, J.; Xiong, F. Early Paleozoic tectonic transition from ocean subduction to collisional orogeny in the Eastern Kunlun region: Evidence from Huxiaoqin mafic rocks. *Acta Petrol. Sin.* **2013**, *29*, 2093–2106.
24. Fu, C.L.; Yan, Z.; Wang, Z.Q.; Buckman, S.; Aitchison, J.C.; Niu, M.L. Lajshankou ophiolite complex: Implications for Paleozoic multiple accretionary and collisional events in the South Qilian belt. *Tectonics* **2019**, *37*, 1321–1346. [[CrossRef](#)]
25. Chen, N.S.; Gong, S.L.; Sun, M.; Li, X.Y.; Xia, X.P.; Wang, Q.Y.; Wu, F.Y.; Xu, P. Precambrian evolution of the Quanji Block, northeastern margin of Tibet: Insights from zircon U-Pb and Lu-Hf isotope compositions. *J. Asian Earth Sci.* **2009**, *35*, 367–376. [[CrossRef](#)]
26. Lu, S.N.; Wang, H.C.; Li, H.K.; Yuan, G.B.; Xin, H.T.; Zheng, J.K. Redefinition of the “Dakendaban Group” on the northern margin of the Qaidam basin. *Geol. Bull. China* **2002**, *21*, 19–23.
27. Lu, S.N.; Chen, Z.H.; Li, H.K.; Hao, G.J.; Zhou, H.Y.; Xiang, Z.Q. Late Mesoproterozoic-early Neoproterozoic evolution of the Qinling orogen. *Geol. Bull. China* **2004**, *23*, 107–112.
28. Wang, H.C.; Lu, S.N.; Mo, X.X.; Li, H.K.; Xin, H.T. An Early Paleozoic collisional orogen on the northern margin of the Qaidam basin, northwestern China. *Geol. Bull. China* **2005**, *24*, 603–612.
29. Song, S.G.; Niu, Y.L.; Zhang, L.F.; Zhang, G.B. Time constraints on orogenesis from oceanic subduction to continental subduction, collision, and exhumation: An example from North Qilian and North Qaidam HP-UHP belts. *Acta Petrol.* **2009**, *25*, 2067–2077.
30. Song, S.G.; Zhang, L.F.; Niu, Y.L. Ultra-deep origin of garnet peridotite from the North Qaidam ultrahigh-pressure belt, northern Tibetan Plateau, NW China. *Am. Mineral.* **2004**, *89*, 1330–1336. [[CrossRef](#)]
31. Song, S.G.; Zhang, L.F.; Niu, Y.L.; Su, L.; Jian, P.; Liu, D.Y. Geochronology of diamond bearing zircons from garnet peridotite in the North Qaidam UHPM belt, northern Tibetan Plateau: A record of complex histories from oceanic lithosphere subduction to continental collision. *Earth Planet. Sci. Lett.* **2005**, *234*, 99–118. [[CrossRef](#)]
32. Li, X.Y.; Chen, N.S.; Xia, X.P.; Sun, M.; Xu, P.; Wang, Q.Y.; Wang, X.Y. Constraints on timing of the early-Paleoproterozoic magmatism and crustal evolution of the Oulongbuluke microcontinent: U-Pb and Lu-Hf isotope systematics of zircons from Mohe granitic pluton. *Acta Petrol.* **2007**, *23*, 513–522.
33. Li, X.C.; Niu, M.L.; Yan, Z.; Wu, Q.; Xia, W.J.; Han, Y.; Da, L.C. SHRIMP Zircon dating for migmatitic biotite plagioclase gneiss from Erlangdong Dakendaban Group in Wulan at the northern margin of Qaidam Basin and its geological significant. *Chin. J. Geol.* **2015**, *50*, 728–740.
34. Li, X.C.; Niu, M.L.; Yakymchuk, C.; Yan, Z.; Fu, C.L.; Zhao, Q.Q. Anatexis of former arc magmatic rocks during oceanic subduction: A case study from the North Wulan gneiss complex. *Gondwana Res.* **2018**, *61*, 128–149. [[CrossRef](#)]
35. Li, X.C.; Niu, M.L.; Yakymchuk, C.; Wu, Q.; Fu, C.L. A paired metamorphic belt in a subduction-to-collision orogen: An example from the South Qilian-North Qaidam orogenic belt, NW China. *J. Metamorph. Geol.* **2019**, *37*, 479–508. [[CrossRef](#)]

36. Wang, L.; Johnston, S.T.; Chen, N.S. New insights into the Precambrian tectonic evolution and continental affinity of the Qilian block: Evidence from geochronology and geochemistry of metasedimentary rocks in the North Wulan terrane. *Geol. Soc. Am. Bull.* **2019**, *131*, 1723–1743. [[CrossRef](#)]
37. Li, C.; Niu, M.L.; Li, X.C.; Yan, Z.; Wu, Q.; Sun, Y.; Yuan, X.Y. Origin and Precambrian paleogeography of the North Wulan terrane, northwestern China: A coherent model of the Tarim-Qilian-Quanji continent during the Columbia-Rodinia supercontinent cycle. *Gondwana Res.* **2022**, *101*, 132–155. [[CrossRef](#)]
38. Yue, Y.; Sun, D.Y.; Hou, K.J.; Peng, Y.B. Geochronology and geochemistry of Triassic gabbro in northern Wulan, northern margin of Qaidam Basin. *J. Jilin Univ.* **2021**, *51*, 154–168.
39. Peng, Y.; Ma, Y.S.; Liu, C.L.; Li, Z.X.; Sun, J.P.; Shao, P.C. Geological characteristics and tectonic significance of the Indosinian granodiorites from the Zongwulong tectonic belt in North Qaidam. *Earth Sci. Front.* **2016**, *23*, 206–221.
40. Gao, J.F.; Lu, J.J.; Lai, M.Y.; Lin, Y.P.; Pu, W. Analysis of trace elements in rock samples using HR-ICPMS. *J. Nanjing Univ.* **2003**, *39*, 844–850.
41. Hanchar, J.M.; Miller, C.F. Zircon zonation patterns as revealed by cathodoluminescence and backscattered electron images—Implications for interpretation of complex crustal histories. *Chem. Geol.* **1993**, *110*, 1–13. [[CrossRef](#)]
42. Pidgeon, R.T. Recrystallisation of oscillatory zoned zircon: Some geochronological and petrological implications. *Contrib. Mineral. Petrol.* **1992**, *110*, 463–472. [[CrossRef](#)]
43. Ludwig, K.R. *Isoplot/Ex Version 2.49. A Geochronological Toolkit for Microsoft Excel*; Berkeley Geochronology Center Special Publication: Berkeley, CA, USA, 2003; pp. 1–56.
44. Middlemost, E.A. Naming materials in the magma/igneous rock system. *Earth Sci. Rev.* **1994**, *37*, 215–224. [[CrossRef](#)]
45. Winchester, J.; Floyd, P. Geochemical discrimination of different magma series and their differentiation products using immobile elements. *Chem. Geol.* **1977**, *20*, 325–343. [[CrossRef](#)]
46. Henderson, P. *Rare Earth Element Geochemistry*; Elsevier: Amsterdam, The Netherlands, 1984; pp. 276–280.
47. Ionow, D.A.; Hofmann, A.W. Nb-Ta-rich mantle amphiboles and micas: Implications for subduction-related metasomatic trace element fractions. *Earth Planet. Sci. Lett.* **1995**, *71*, 241–262.
48. Kelemen, P.B.; Hanghij, K.; Greene, A.R. One view of the geochemical of subduction-related magmatic arcs, with an emphasis primitive andesite and lower crustal. *Treatise Geochem.* **2007**, *138*, 659–670.
49. Taylor, S.R.; McLennan, S.M. *The Continental Crust: Its Composition and Evolution*; Blackwell: Oxford, UK, 1985; pp. 1–62.
50. Sun, S.S.; McDonough, W.F. Chemical and isotopic systematics of oceanic basalts: Implications for mantle composition and processes. *Geol. Soc. Lond. Spéc. Publ.* **1989**, *42*, 313–345. [[CrossRef](#)]
51. Belousova, E.A.; Griffin, W.L.; Pearson, N.J. Trace element composition and cathodoluminescence properties of southern African kimberlitic zircons. *Miner. Mag.* **1998**, *62*, 355–366. [[CrossRef](#)]
52. Belousova, E.A.; Griffin, W.L.; O'Reilly, S.Y. Zircon crystal morphology, trace element signatures and Hf isotope composition as a tool for petrogenetic modelling: Examples from Eastern Australian granitoids. *J. Pet.* **2005**, *47*, 329–353. [[CrossRef](#)]
53. Belousova, E.A.; Griffin, W.L.; O'Reilly, S.Y.; Fisher, N. Igneous zircon: Trace element composition as an indicator of source rock type. *Contrib. Mineral. Pet.* **2002**, *143*, 602–622. [[CrossRef](#)]
54. Kirkland, C.L.; Smithies, R.; Taylor, R.; Evans, N.; McDonald, B. Zircon Th/U ratios in magmatic environs. *Lithos* **2015**, *212*, 397–414. [[CrossRef](#)]
55. Cavosie, A.J.; Kita, N.T.; Valley, J.W. Primitive oxygen-isotope ratio recorded in magmatic zircon from the Mid-Atlantic Ridge. *Am. Mineral.* **2009**, *94*, 926–934. [[CrossRef](#)]
56. Kinny, P.D.; Wijbrans, J.R.; Froude, D.O.; Williams, I.S.; Compston, W. Age constraints on the geological evolution of the Narryer Gneiss Complex, Western Australia. *Aust. J. Earth Sci.* **1990**, *37*, 51–69. [[CrossRef](#)]
57. DePaolo, D.J. Trace element and isotopic effects of combined wallrock assimilation and fractional crystallization. *Earth Planet. Sci. Lett.* **1981**, *53*, 189–202. [[CrossRef](#)]
58. Halama, R.; Marks, M.; Brüggemann, G.; Siebel, W.; Wenzel, T.; Markl, G. Crustal contamination of mafic magmas: Evidence from a petrological, geochemical and Sr-Nd-Os-O isotopic study of the Proterozoic Isortoq dike swarm, South Greenland. *Lithos* **2004**, *74*, 199–232. [[CrossRef](#)]
59. Mir, A.R.; Alvi, S.H.; Balaram, V. Geochemistry of the mafic dykes in parts of the Singhbhum granitoid complex: Petrogenesis and tectonic setting. *Arab. J. Geosci.* **2010**, *4*, 933–943. [[CrossRef](#)]
60. Hofmann, A.W.; Jochum, K.P.; Seufert, M.; White, W.M. Nb and Pb in oceanic basalts: New constraints on mantle evolution. *Earth Planet. Sci. Lett.* **1986**, *79*, 33–45. [[CrossRef](#)]
61. Müunker, C.; Pfander, J.A.; Weyer, S.; Buchl, A.; Kleine, T.; Mezger, K. Evolution of planetary cores and the Earth-Moon system from Nb/Ta systematics. *Science* **2003**, *301*, 84–88. [[CrossRef](#)]
62. Barth, M.G.; McDonough, W.F.; Rudnick, R.L. Tracking the budget of Nb and Ta in the continental crust. *Chem. Geol.* **2000**, *165*, 197–213. [[CrossRef](#)]
63. Zhao, J.H.; Zhou, M.F. Geochemistry of Neoproterozoic mafic intrusions in the Panzhihua district (Sichuan Province, SW China): Implications for subduction-related metasomatism in the upper mantle. *Precambrian Res.* **2007**, *152*, 27–47. [[CrossRef](#)]
64. Sklyarov, E.V.; Gladkochub, D.; Mazukabzov, A.; Menshagin, Y.; Watanabe, T.; Pisarevsky, S. Neoproterozoic mafic dike swarms of the Sharyzhalgai metamorphic massif, southern Siberian craton. *Precambrian Res.* **2003**, *122*, 359–376. [[CrossRef](#)]

65. Wendlandt, R.F.; Ahherr, R.; Neumann, E.R.; Baldrige, W.S. *Petrology, Geochemistry, Isotopes. Continental Rifts: Evolution, Structure, Tectonics*; Elsevier: Amsterdam, The Netherlands, 1995; pp. 47–60.
66. Ringwood, A.E. The petrological evolution of island arc systems (Twenty-seventh William Smith Lecture). *J. Geol. Soc.* **1974**, *130*, 183–204. [[CrossRef](#)]
67. Jahn, B.M.; Wu, F.Y.; Lo, C.H.; Tsai, C.H. Crust-mantle interaction induced by deep subduction of the continental crust: Geochemical and Sr-Nd isotopic evidence from post-collisional mafic-ultramafic intrusions of the northern Dabie complex, central China. *Chem. Geol.* **1999**, *157*, 119–146. [[CrossRef](#)]
68. Gill, J.B. *Orogenic Andesites and Plate Tectonics*; Springer: New York, NY, USA, 1981; pp. 1–385.
69. Pearce, J.A.; Peate, D.W. Tectonic implications of the composition of volcanic arc magmas. *Annu. Rev. Earth Planet Sci.* **1995**, *23*, 251–285. [[CrossRef](#)]
70. Miller, D.M.; Goldstein, S.L.; Langmuir, C.H. Cerium/lead and lead isotope ratios in arc magmas and the enrichment of lead in the continents. *Nature* **1994**, *368*, 514–520. [[CrossRef](#)]
71. Turner, S.; Hawkesworth, C.; Rogers, N.; Bartlett, J.; Worthington, T.; Hergt, J.; Pearce, J.; Smith, I.  $^{238}\text{U}/^{230}\text{Th}$  disequilibria, magma petrogenesis, and flux rates beneath the depleted Tonga-Kermadec island arc. *Geochim. Et Cosmochim. Acta* **1997**, *61*, 4855–4884. [[CrossRef](#)]
72. Class, C.; Miller, D.M.; Goldstein, S.L.; Langmuir, C.H. Distinguishing melt and fluid subduction components in Umnak Volcanics, Aleutian Arc. *Geochem. Geophys. Axed Geosystems* **2000**, *1*, 1044. [[CrossRef](#)]
73. Hochstaedter, A.; Gill, J.; Peters, R.; Broun, P.; Holden, P.; Taylor, B. Across-arc geochemical in the Izu-Bonin arc: Contributions from the subducting slab. *Geochem. Geophys. Geosystems* **2001**, *2*, 1019–1029. [[CrossRef](#)]
74. Seghedi, I.; Downes, H.; Pécskay, Z.; Thirlwall, M.F.; Szakas, A.; Prychodko, M.; Matthey, D. Magmagenesis in a subduction-related poses collisional volcanic arc segment: The Ukrainian Carpathians. *Lithos* **2001**, *57*, 237–262. [[CrossRef](#)]
75. Guo, Z.; Wilson, M.; Liu, J. Post-collisional, potassic and ultrapotassic magmatism of the northern Tibetan plateau: Constraints on characteristics of the mantle source, geodynamic setting and uplift mechanisms. *J. Petrol.* **2006**, *47*, 1177–1220. [[CrossRef](#)]
76. Elliott, T.; Plank, T.; Zindler, A.; White, W.; Bourdon, B. Element transport from slab to volcanic front at the Mariana arc. *J. Geophys. Res.* **1997**, *102*, 14991–15019. [[CrossRef](#)]
77. Ayers, J. Trace element modeling of aqueous fluid-peridotite interaction in the mantle wedge of subduction zones. *Contrib. Mineral. Petrol.* **1998**, *132*, 394–404. [[CrossRef](#)]
78. Ishikawa, T.; Tera, F. Two isotopically distinct fluid components involved in the Mariana Arc: Evidence from Nb/B ratios and B, Sr, Nd and Pb isotope systematics. *Geology* **1999**, *27*, 83–86. [[CrossRef](#)]
79. Guo, Z.F.; Hertogen, J.; Liu, J.Q.; Pasteels, P.; Boven, A.; Punzalan, L.; He, H.Y.; Luo, X.J.; Zhang, W.H. Potassic magmatism in Western Sichuan and Yunnan provinces, SE Tibet, China: Petrological and geochemical constraints on petrogenesis. *J. Petrol.* **2005**, *46*, 33–78. [[CrossRef](#)]
80. Tian, L.; Castillo, P.R.; Hilton, D.R.; Hawkins, J.W.; Hanan, B.B.; Pietruszka, A.J. Major and trace element and Sr-Nd isotope signatures of the northern Lau Basin lavas: Implications for the composition and dynamics of the back-arc basin mantle. *J. Geophys. Res. Space Phys.* **2008**, *178*, 657–670. [[CrossRef](#)]
81. Woodhead, J.; Hergt, J.M.; Davidson, J.; Eggins, S. Hafnium isotope evidence for ‘conservative’ element mobility during subduction zone processes. *Earth Planet. Sci. Lett.* **2001**, *192*, 331–346. [[CrossRef](#)]
82. Hoffer, G.; Eissen, J.P.; Beate, B.; Bourdon, E.; Fornari, M.; Cotton, J. Geochemical and petrological constraints on rear-arc magma genesis processes in Ecuador: The Puyo cones and Mera lavas volcanic formations. *J. Volcanol. Geotherm. Res.* **2008**, *176*, 107–118. [[CrossRef](#)]
83. Wood, D.A. The application of a Th-Hf-Ta diagram to problems of tectonomagmatic classification and to establishing the nature of crustal contamination of basaltic lavas of the British Tertiary Volcanic Province. *Earth Planet. Sci. Lett.* **1980**, *50*, 11–30. [[CrossRef](#)]
84. Pearce, J.A. Geochemical fingerprinting of oceanic basalts with applications to ophiolite classification and the search for Archean oceanic crust. *Lithos* **2008**, *100*, 14–48. [[CrossRef](#)]
85. Fu, C.L.; Yan, Z.; Guo, X.Q.; Niu, M.L.; Chen, L.; Xia, W.J. Magma source and tectonic setting of the granitoids associated with Saishitang Cu deposit in the West Qinling terrane. *Acta Petrol. Sin.* **2016**, *32*, 1997–2014.
86. Gu, P.Y.; Chen, R.M.; Zha, X.F.; Dong, Z.C.; Zhuang, Y.J.; Zhang, F.Y.; Li, P.Q. The age, petrogenesis and geological significance of quartz diorite on the northwestern margin of Qaidam basin. *Acta Petrol. Mineral.* **2018**, *37*, 19–33.
87. Dong, Z.C.; Gu, P.Y.; Chen, R.M.; Zha, X.F.; Zhang, H.D. Geochronology, geochemistry, and Hf isotope of Yanchangbeishan adamellite of Lenghu area in Qinghai. *Earth Sci.* **2015**, *40*, 130–144.
88. Dong, Z.C.; Yang, C.; Gu, P.Y.; Wang, H.; Zha, X.F.; Chen, R.M.; Zhang, H.D. Chronology and geochemistry of Yanchangbeishan biotite adamellite of Lenghu area in Qinghai and the geological significance. *Geotecton. Metallog.* **2015**, *39*, 167–178.
89. Wang, S.; Feng, C.Y.; Li, S.J.; Jiang, J.H.; Li, D.S.; Su, S.S. Zircon SHRIMP U-Pb dating of granodiorite in the Kaerqueka polymetallic ore deposit, Qimantage Mountain, Qinghai Province, and its geological implications. *Geol. China* **2009**, *36*, 74–84.

**Disclaimer/Publisher’s Note:** The statements, opinions and data contained in all publications are solely those of the individual author(s) and contributor(s) and not of MDPI and/or the editor(s). MDPI and/or the editor(s) disclaim responsibility for any injury to people or property resulting from any ideas, methods, instructions or products referred to in the content.